The Journal of Immunology

Niclosamide Prevents Systemic Sclerosis in a Reactive Oxygen Species–Induced Mouse Model

Florence Morin, Niloufar Kavian, Carole Nicco, Olivier Cerles, Christiane Chéreau and Frédéric Batteux

J Immunol 2016; 197:3018-3028; Prepublished online 9 September 2016;
doi: 10.4049/jimmunol.1502482
http://www.jimmunol.org/content/197/8/3018

The Journal of Immunology is published twice each month by
The American Association of Immunologists, Inc.,
1451 Rockville Pike, Suite 650, Rockville, MD 20852

Print ISSN: 0022-1767 Online ISSN: 1550-6606.

Niclosamide Prevents Systemic Sclerosis in a Reactive Oxygen Species–Induced Mouse Model

Florence Morin,*,† Niloufar Kavian,*,† Carole Nicco,* Olivier Cerles,* Christiane Chéreau,* and Frédéric Batteux*,†

Systemic sclerosis (SSc) is a connective tissue disorder characterized by fibrosis of the skin and inner organs, vasculopathy, and immunological abnormalities. Recent insights on the implication of STAT3, AKT, and Wnt/β-catenin in fibrosis have prompted us to investigate, in a mouse model of ROS-induced SSc, the effects of niclosamide, an antihelmintic drug that inhibits both of these signaling pathways. SSc was induced in BALB/c mice by daily s.c. injections of hypochlorous acid (HOCl). Mice were treated or not every other day, 5 d a week, for 6 wk, by niclosamide. Skin and lung fibrosis as well as immunological features were studied. Mice exposed to HOCl developed a diffuse cutaneous SSc with pulmonary fibrosis and anti-DNA topoisomerase 1 autoantibodies. STAT3, AKT, and Wnt/β-catenin pathways were hyperactivated in the skin and the lungs of diseased mice. Niclosamide reversed fibrosis of the skin and the lungs. Beneficial immunological effects were also observed because niclosamide decreased the activation of $CD4^+$ and $CD8^+$ T cells, autoimmune B cell activation, as well as IL-4 and IL-13 production in the skin. The improvement permitted by niclosamide in the mouse model of HOCl-induced SSc as well as the well-documented safety profile of this drug provide a rationale for the evaluation of niclosamide in the management of patients affected by this disease. *The Journal of Immunology*, **2016, 197: 3018–3028.**

Systemic sclerosis (SSc) is a connective tissue disorder characterized by fibrosis of the skin and inner organs, vascular alterations, and dysimmunity including the presence of autoantibodies to nuclear proteins (1). The cause of this disease remains unknown, and its understanding is further complicated by its inherent heterogenous clinical manifestations (2). Vascular dysfunction can precede the disease by several years (3). Fibrosis is the result of an accumulation of extracellular matrix in the skin and inner organs produced by myofibroblasts that express smooth muscle cell markers such as α-smooth muscle actin (α-SMA) (4, 5). This process is triggered by an initial tissue injury that leads to the production of vasoactive mediators, free radicals, and inflammatory cytokines that, in turn, activate endothelial, fibroblastic, and immune cells (6). Over the past few years, the role of activated B cells in fibrosis has been emphasized. In addition to autoantibody production, these can directly activate fibroblasts (7). Regarding T cells, skin infiltration by $CD4^+$ T cells appears in the early stage of the disease and the production of Th2 cytokines such as IL-4 and IL-13 promotes fibroblast activation (8, 9). Thus, the pathophysiology of SSc results from complex interactions among endothelial cells, fibroblasts, and immune cells. Although progress has been made in the treatment of some of the visceral complications, to date no treatment is available to cure SSc, mainly because most of the mechanisms underlying the disease remain unclear (10, 11).

Niclosamide or 5-chloro-*N*-(2-chloro-4-nitrophenyl)-2-hydroxybenzamide is an antihelmintic drug used to treat cestode and threadworm infections (12). Recently, several groups have independently reported that niclosamide is active against certain solid cancers (13–15). This drug acts through different signaling pathways such as STAT3 and Wnt/β-catenin pathways: niclosamide inhibits nuclear translocation and transcriptional activity of STAT3, and also inhibits β-catenin stabilization and β-catenin/TCF transcription-activating complex (16). STAT3 is a member of STAT proteins, which play critical roles in several cell functions such as proliferation, migration, survival, and differentiation (17). This protein is also a downstream signaling mediator of the inflammatory cytokine IL-6 (18) and has been identified as an intracellular mediator for the profibrotic effects of TGF-β in fibroblasts (19). Wnt proteins are a family of 19 proteins playing essential roles in processes such as differentiation, proliferation, and migration. They modulate two signaling pathways: the canonical (β-catenin–dependent) and the noncanonical (β-catenin–independent) pathways (20). The Wnt/β-catenin pathway, implicated in wound healing (21), has been linked to the regulation of fibrogenesis (22, 23). This signaling pathway is involved in patients with SSc because it is overexpressed in human skin where it activates fibroblasts and promotes their differentiation into myofibroblasts (24, 25). Furthermore, the AKT signaling pathway seems to be implicated in fibrosis because its inhibition can reduce collagen production by human fibroblasts (26, 27). Moreover, this pathway can affect β-catenin by inhibiting GSK3β and stabilizing β-catenin (28, 29).

We were therefore prompted to investigate the effects of niclosamide, a coinhibitor of STAT3, AKT, and Wnt/β-catenin pathways, in an ROS-induced mouse model of SSc.

Materials and Methods

Animals and chemicals

Six-week-old female BALB/c mice were purchased from Janvier Laboratory (Le Genest Saint Isle, France). Animals received humane care in

*Institut Cochin, INSERM U1016, CNRS, UMR8104, Université Paris Descartes, Université Sorbonne Paris Cité, 75014 Paris, France; and †Laboratoire d'Immunologie Biologique, Hôpital Cochin, Assistance Publique-Hopitaux de Paris, 75679 Paris Cedex 14, France

ORCID: 0000-0001-5697-7484 (O.C.).

Received for publication November 25, 2015. Accepted for publication August 14, 2016.

This work was supported by grants from the Institut Cochin.

Address correspondence and reprint requests to Prof. Frédéric Batteux, Laboratoire d'Immunologie, INSERM U1016, Institut Cochin, 8 rue Méchain, 75679 Paris Cedex 14, France. E-mail address: frederic.batteux@aphp.fr

The online version of this article contains supplemental material.

Abbreviations used in this article: AU, arbitrary unit; HOCl, hypochlorous acid; SMA, smooth muscle actin; SSc, systemic sclerosis.

compliance with the guidelines implemented at our institution (INSERM and Université Paris Descartes, Ethics committee CEEA 34, protocol CEEA34.CN.023.11). All mice were housed in ventilated cages with sterile food and water ad libitum. All chemicals were obtained from Sigma-Aldrich.

Induction of SSc by intradermal injections of hypochlorous acid solution

Mice were randomly distributed into experimental and control groups (10 mice/group). SSc was induced according to the protocol described by Kavian et al. (30). A total of 400 μl of an hypochlorous acid (HOCl) solution was prepared extemporaneously and injected intradermally into the shaved backs of mice (one injection of 200 μl in each flank), using a 27-gauge needle, every day for 6 wk (HOCl-mice). HOCl was prepared by adding a NaClO solution (9.6% active chlorine) to 100 mM of KH2PO4 (pH 6.2) (31). HOCl concentration was assessed by measuring the OD of the solution at 280 nm, which was then adjusted to an OD between 0.7 and 0.9. Control mice received injections of 400 μl of sterilized PBS (PBS-mice).

Induction of SSc with bleomycin

Mice were randomly distributed into experimental and control groups (10 mice per group). Mice developed bleomycin-induced SSc after daily intradermal injections using a 27-gauge needle of 100 μl of bleomycin (100 mg/ml) in PBS, for 6 wk (bleomycin-mice). Control mice received injections of 100 μl of sterilized PBS (PBS-mice).

Treatment of HOCl-mice and bleomycin-mice with niclosamide

HOCl-, bleomycin-, and PBS-mice were randomized and treated every other day 5 d a week for 6 wk with either niclosamide (10 mg/kg by i.p. injections) or vehicle (DMSO 5%) alone (10 mice/group) (15). Stock solution of niclosamide (2 mg/ml in DMSO) was prepared and kept at −20°C. A 1:20 dilution of this solution was prepared immediately before injection. Animals were sacrificed by cervical dislocation after 6 wk.

Dermal thickness assessment

One day before mice were killed, skin thickness of the shaved backs of mice was measured with a caliper and expressed in millimeters.

Histopathological analysis

Fixed skin and lung samples were embedded in paraffin. A 5-μm-thick tissue section was stained with H&E or with Masson's trichrome staining (Kit Trichrome de Masson; RAL Diagnostics, Martillac, France). Slides were examined by standard brightfield microscopy (Nikon Eclipse 80i, Tokyo, Japan) by a pathologist who was blinded to the experimental group assignment. Quantitative assessment of collagen on trichrome-stained slides was performed with ImageJ software.

Immunohistochemistry of lung tissue section

Expression of α-SMA and β-catenin was assessed by immunohistochemistry of lung fragments derived from HOCl and PBS mice treated or not with niclosamide. Tissue sections were deparaffinized and rehydrated, and then incubated with 200 μg/ml proteinase K for 15 min at 37°C for Ag retrieval. Specimens were then treated with 3% v/v H_2O_2 for 10 min at 37°C to inhibit endogenous peroxidases and then blocked with 5% w/v BSA for 1 h at 4°C. Sections were incubated with 1:100 anti–α-SMA, mAb conjugated with alkaline phosphatase (A5691; Sigma-Aldrich), and a 1:100 mAb directed to β-catenin (610154; BD Biosciences, San Jose, CA) overnight at 4°C. Sections incubated with β-catenin were then incubated with HRP-conjugated secondary goat anti-rabbit Ab (Dako) for 1 h at room temperature. Ab binding for α-SMA staining was visualized by using NBT chloride/5-bromo-4-chloro-3-indolyl phosphate. Staining of β-catenin was visualized by using diaminobenzidine tetrahydrochloride as a chromogen. Only slides incubated with β-catenin were stained with hematoxylin. All slides were examined with standard brightfield microscopy (Nikon Eclipse 80i). Appropriate controls with irrelevant alkaline phosphatase–conjugated and HRP-conjugated Abs were performed.

Collagen content in skin and lung

Punch biopsies (6-mm diameter) from the skin and lung samples of each mouse were weighted, dilacerated using a scalpel, put into tubes, thawed, and mixed with pepsin (1:10 weight ratio) and 0.5 M acetic acid overnight at room temperature under stirring. The assay of collagen content was based on the quantitative dye-binding Sircol method (Biocolor, Belfast, U.K.).

Hydroxyproline content in skin and lung

After digestion of punch biopsies (3-mm diameter) in HCl (6 M) for 3 h at 120°C, the pH of the samples was adjusted to 7. Samples were then mixed with chloramine T (0.06 M) and incubated for 20 min at room temperature. Perchloric acid (3.15 M) and *p*-dimethylaminobenzaldehyde (20%) were then added and samples were incubated for an additional 20 min at 60°C. The absorbance was determined at 557 nm with a microplate spectrophotometer (Fusion; PerkinElmer, Wellesley, MA).

Determination of cutaneous IL-4 and IL-13 production

Punch biopsies (6-mm diameter) from the skin and a weighted lobe of lung of each mouse were incubated for 72 h at 37°C in complete RPMI 1640 medium with 5 μg/ml Con A in a total volume of 1 ml. Supernatants were collected and immediately frozen at −80°C. Cytokine concentrations in the 1:4 diluted supernatants were measured by ELISA, as previously described (32). Mouse IL-4 ELISA Ready-SET-Go!, Mouse IL-13 ELISA Ready-SET-Go!, and Mouse IL-6 ELISA Ready-SET-Go! kits were purchased from eBioscience (San Diego, CA). Concentrations were measured, before being calculated from a standard curve according to the manufacturer's protocol. Results were expressed in picograms per milliliter. For lung samples, the concentrations found in the lungs were reported to the weight of the selected lobe and adjusted to 1 mg of lung.

Western blot of p-STAT3, STAT3, p-AKT, AKT, β-catenin, and α-SMA proteins in the skin and lungs

Skin and lung fragments were incubated with 100 μl of radioimmunoprecipitation assay buffer for Western blot. Protein extracts (30 μg of total protein) were resolved by 10% SDS-PAGE and were blotted to nitrocellulose membranes. Blots were blocked with 5% nonfat milk and incubated overnight at 4°C with a 1:1000 rabbit polyclonal anti–phospho-STAT3 (Tyr^{705}) (9131; Cell Signaling, Danvers, MA), a 1:200 rabbit polyclonal anti-STAT3 (K-15) (sc-483; Santa Cruz Biotechnology, Dallas, TX), a 1:1000 rabbit polyclonal anti–phospho-AKT (Ser^{473}) (9271; Cell Signaling), a 1:1000 rabbit polyclonal anti-AKT (9272; Cell Signaling), a 1:1000 mouse polyclonal anti–β-catenin (610154; BD Biosciences), or a 1:50,000 mouse monoclonal anti–α-SMA (A 5228; Sigma-Aldrich). Signals were developed using a 1:1000 goat anti-rabbit HRP-conjugated secondary Ab or a 1:1000 goat anti-mouse HRP-conjugated secondary Ab (Dako, Glostrup, Denmark). Immunoreactivities were revealed using ECL (Amersham, Switzerland), and densitometric analyses were performed using ImageJ software. Results were expressed as arbitrary units (AU), defined as the densitometric intensity of the bands of the proteins tested divided by the densitometric intensity of the same bands labeled with mouse anti–β-actin mAb.

Flow cytometric analysis of spleen cell subsets

Cell suspensions from spleens were prepared after hypotonic lysis of erythrocytes in potassium acetate solution. For each mouse, splenocytes were counted with Malassez cell. Cells were incubated with the appropriate labeled Ab at 4°C for 30 min in PBS with 2% normal FCS. Flow cytometry was performed using a FACS Canto II flow cytometer (BD Biosciences), according to standard techniques. The mAbs used in this study were anti–CD3-FITC, anti–CD4-BV421, anti–CD8-PE-Cy7, anti–CD69-PE, and anti–B220-allophycocyanin mAbs on one hand, and anti–B220-allophycocyanin, anti–CD21-FITC, anti–CD23-PE, anti–IgM-biotin and streptavidin-PerCP-Cy5.5, anti–CD93-PE-Cy7, and anti–CD43-BV421 (BD Biosciences) mAbs on the other hand. Data were analyzed with FlowJo software (Tree Star, Ashland, OR).

Assays of anti-DNA topoisomerase 1 autoantibodies in sera

Levels of anti-DNA topoisomerase 1 IgG Abs were detected by ELISA using purified calf thymus DNA topoisomerase 1 bound to the wells of a microtiter plate (Abnova, Taiwan). A 1:4 mouse serum dilution and a 1:1000 anti-murine Ig HRP (Dako) secondary Ab dilution were used as previously described (33).

Statistical analysis

All quantitative data were expressed as means ± SEM. Data were compared using one-way ANOVA followed by a Dunn multiple comparison test. Student unpaired *t* test was used to compare two groups. All

analyses were carried out using the GraphPad Prism 5.0 statistical software package (San Diego, CA), and p values <0.05 were considered significant.

Results

Effects of niclosamide on skin fibrosis and cytokine production in HOCl-mice

One day before sacrifice, HOCl-mice exhibited a thicker skin than PBS-mice (1.60 ± 0.05 versus 0.55 ± 0.03 mm, $p < 0.0001$; Fig. 1A). Treated HOCl-mice groups showed a thinner skin compared with untreated ones (0.92 ± 0.02 versus 1.60 ± 0.05 mm, $p < 0.0001$; Fig. 1A). Pathological analysis confirmed that HOCl-mice had a thicker skin than PBS-mice (Fig. 1B). Skin thickening was reduced in niclosamide-treated HOCl-mice compared with untreated HOCl-animals (Fig. 1B). Skin collagen content, assessed by Sirius red assay, was increased in HOCl-mice compared with PBS-mice (33.3 ± 0.7 versus 1.30 ± 1.8 μg/punch, $p < 0.0001$; Fig. 1C). Collagen content was lower in the skin of niclosamide-treated HOCl-mice than in untreated HOCl-animals (20.0 ± 1.1 versus 33.3 ± 0.7 μg/punch, $p < 0.0001$; Fig. 1C). Semiquantitative assessment of Masson's trichrome staining confirmed the increased collagen content in the skin of HOCl-mice compared with PBS-mice (58.12 ± 2.14 versus 42.96 ± 1.22% skin collagen, $p = 0.0026$; Fig. 1D). Niclosamide-treated HOCl-mice present a lower amount of collagen in the skin than untreated HOCl-mice (47.55 ± 2.24 versus 58.12 ± 2.14% skin collagen, $p = 0.0220$; Fig. 1D). Cytokine production was measured in the skin by ELISA. We found increased levels of IL-4 in diseased mice compared with healthy mice (1619 ± 460 versus 143 ± 87 pg/ml, $p = 0.0264$; Fig. 1F). Treatment by niclosamide reduced IL-4 production in the skin of HOCl-mice compared with untreated mice (430 ± 186 versus 1619 ± 460 pg/ml, $p = 0.0177$; Fig. 1F). Similarly, IL-13 production in the skin of HOCl-mice was higher than in control mice (7159 ± 1528 versus 1548 ± 297 pg/ml, $p = 0.0410$; Fig. 1G). HOCl-injected and niclosamide-treated mice had a lower production of IL-13 in the skin than diseased HOCl-mice (1753 ± 452 versus 7159 ± 1528 pg/ml, $p = 0.0023$; Fig. 1G).

Effects of niclosamide on skin fibrosis, cytokine production, and expression of α-SMA and β-catenin in bleomycin-mice

We observed a thickening of the skin of bleomycin-injected mice compared with control mice (1.36 ± 0.07 versus 0.79 ± 0.03 mm, $p < 0.0001$; Supplemental Fig. 1A). Treatment with niclosamide reduced this thickening in bleomycin-mice (0.89 ± 0.02 versus 1.36 ± 0.07 mm, $p < 0.0001$; Supplemental Fig. 1A). Collagen evaluation using the hydroxyproline method in the skin revealed an increased production of collagen in bleomycin-mice compared with PBS-mice (184.5 ± 9.0 versus 138.8 ± 10.3 μg/punch, $p = 0.0264$; Supplemental Fig. 1B). The production of hydroxyproline was lower in niclosamide-treated bleomycin-mice than in untreated bleomycin-mice (140.8 ± 5.6 versus 184.5 ± 9.0 μg/punch, $p = 0.0015$; Supplemental Fig. 1B). Also, we measured the levels of IL-4 and IL-13 in the skin with the same method used in the HOCl-induced mouse model of SSc. We found higher levels of these two cytokines in the skin of bleomycin-mice than in PBS-mice (IL-4: 114.6 ± 42.6 versus 1.0 ± 0.1 pg/ml, $p = 0.0354$, Supplemental Fig. 1C; IL-13: 502.8 ± 159 versus 58.5 ± 7.4 pg/ml, $p = 0.0090$, Supplemental Fig. 1D). Treatment with niclosamide reduced the production of IL-4 and IL-13 in the skin of bleomycin-mice compared with untreated ones (IL-4: 1.2 ± 0.2 versus 114.6 ± 42.6 pg/ml, $p = 0.0358$, Supplemental Fig. 1C; IL-13: 59.7 ± 6.6 versus 502.8 ± 159 pg/ml, $p = 0.0091$, Supplemental Fig. 1D). Finally, we performed Western blot to measure the expression of α-SMA and β-catenin in the skin. In bleomycin-mice, we found a higher expression of these proteins than in PBS-mice (α-SMA: 1.49 ± 0.14 versus 0.85 ± 0.03 AU, $p = 0.0396$, Supplemental Fig. 1F; β-catenin: 1.75 ± 0.33 versus 0.67 ± 0.09 AU, $p = 0.0396$, Supplemental Fig. 1G). Niclosamide decreased expression of α-SMA and β-catenin in the skin of bleomycin-mice compared with untreated bleomycin-mice (α-SMA: 0.62 ± 0.07 versus 1.49 ± 0.14 AU, $p = 0.0015$, Supplemental Fig. 1F; β-catenin: 0.62 ± 0.11 versus 1.75 ± 0.33 AU, $p = 0.0163$, Supplemental Fig. 1G).

Effects of niclosamide on lung fibrosis and expression of α-SMA and β-catenin in the lungs

An increased amount of collagen was observed in the lungs of HOCl-mice compared with PBS-mice (5.40 ± 0.57 versus 3.59 ± 0.42 μg/g of lung, $p = 0.0437$; Fig. 2A). Niclosamide-treated HOCl-mice presented a lower content of collagen than untreated HOCl-mice (3.32 ± 0.21 versus 5.40 ± 0.57 μg/g of lung, $p = 0.0027$; Fig. 2A). Indeed, histological examination of the lungs from HOCl-mice with H&E staining revealed an alveolar luminal narrowing and a thickening of connective tissues (Fig. 2B). Niclosamide improved these pathological features in HOCl-mice. Semiquantitative assessment of Masson's trichrome staining confirmed the increased collagen content in the lungs of HOCl-mice compared with PBS-mice (41.60 ± 4.66 versus 16.14 ± 10.58% lung collagen, $p = 0.0265$; Fig. 2C). Niclosamide-treated HOCl-mice present a lower amount of collagen in the lungs than untreated HOCl-mice (12.56 ± 9.42 versus 41.60 ± 4.66% lung collagen, $p = 0.0077$; Fig. 2C). Moreover, we found an increased expression of α-SMA and β-catenin in the lungs of HOCl-mice (Fig. 2E, 2F). These abnormal expressions were abrogated by niclosamide.

Effect of niclosamide on the engagement of STAT3, AKT, and Wnt/β-catenin pathways in the skin of HOCl-mice

p-STAT3 expression was higher in the skin of HOCl-mice than in PBS-mice (1.34 ± 0.44 versus 0.14 ± 0.04 AU, $p = 0.0159$; Fig. 3A, 3B). Niclosamide significantly decreased the expression of pSTAT3 in HOCl-mice compared with untreated HOCl-mice (0.32 ± 0.05 versus 1.34 ± 0.44 AU, $p = 0.0063$; Fig. 3A, 3B). We found an increased expression of the phosphorylated form of AKT in the skin of HOCl-mice compared with PBS-mice (0.84 ± 0.149 versus 0.37 ± 0.05 AU, $p = 0.0404$; Fig. 3A, 3C). Treatment with niclosamide reduced the expression of p-AKT in the skin of HOCl-mice compared with untreated mice (0.31 ± 0.07 versus 0.84 ± 0.14 AU, $p = 0.0316$; Fig. 3A, 3C). Similarly, the expression of β-catenin was higher in the skin of HOCl-mice than in PBS-mice (0.75 ± 0.15 versus 0.12 ± 0.02 AU, $p = 0.0339$; Fig. 3A, 3D). Niclosamide decreased the expression of β-catenin in HOCl-animals (0.30 ± 0.06 versus 0.75 ± 0.15 AU, $p = 0.0063$; Fig. 3A, 3D). Furthermore, the expression of α-SMA was higher in the skin of HOCl-mice than in PBS-mice (2.30 ± 0.44 versus 0.32 ± 0.08 AU, $p = 0.0116$; Fig. 3A, 3E). Niclosamide also decreased the expression of α-SMA in HOCl-mice compared with untreated animals (0.89 ± 0.11 versus 2.30 ± 0.44 AU, $p = 0039$; Fig. 3A, 3E). Moreover, IL-6 production was higher in the skin of HOCl-injected mice than in control mice (6315 ± 323 versus 4808 ± 524 pg/ml, $p = 0.0374$; Fig. 3F). Treatment with niclosamide reduced its levels in HOCl-mice (5071 ± 411 versus 6315 ± 323 pg/ml, $p = 0.0444$; Fig. 3F).

Implication of STAT3, AKT, and Wnt pathways in lung fibrosis and effect of niclosamide

In the lungs, expression of the p-STAT3 was increased in HOCl-mice (5.46 ± 2.50 versus 0.36 ± 0.09 AU, $p = 0.0469$; Fig. 4A, 4B).

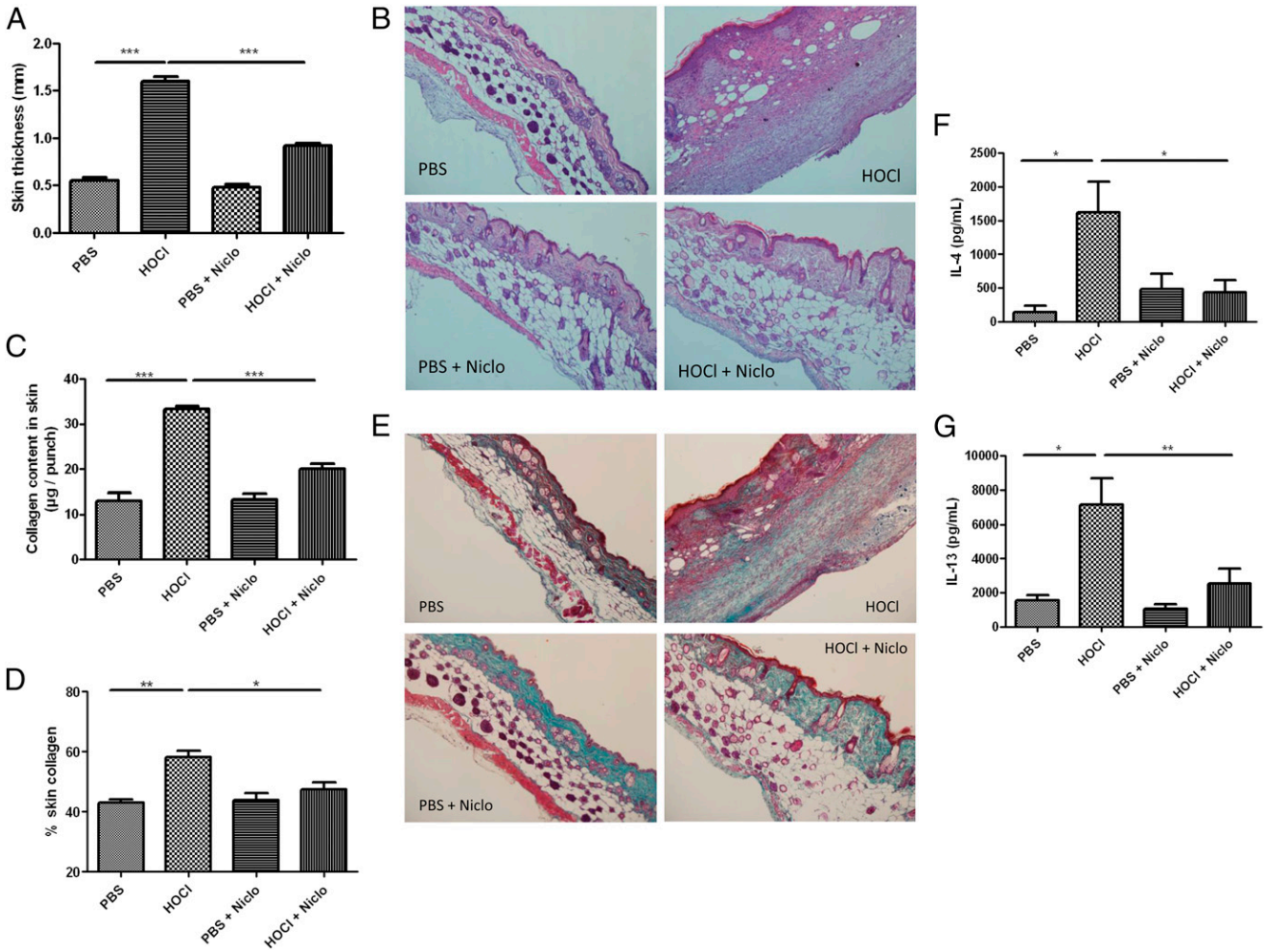

FIGURE 1. Cutaneous effects of niclosamide in mice with HOCl-induced SSc. (**A**) Skin thickness measurement after niclosamide treatment (measurement was performed 1 d before killing). (**B**) Thickness of skin in PBS-mice and HOCl-mice, treated or not with niclosamide. Representative sections of 5 μm. (**C**) Collagen content in the skin of mice expressed in milligrams per punch biopsy. (**D**) Collagen content in the skin of mice assessed histologically with ImageJ. (**E**) Representative 5-μm-thick sections of skin from PBS-mice and HOCl-mice, treated or not with niclosamide stained with Masson's trichrome. (**F**) Levels of IL-4 in the skin. (**G**) Levels of IL-13 in the skin. Photographs were taken with a Nikon Eclipse 80i microscope. Original magnification ×50. Ten mice per group representative of two experiments. (A, C, D, F, and G) Values are means ± SEM. $*p \leq 0.05$, $**p \leq 0.01$, $***p \leq 0.001$.

Treatment by niclosamide decreased the expression of p-STAT3 in HOCl-mice compared with untreated mice (0.31 ± 0.07 versus 5.46 ± 2.50 AU, $p = 0.0331$; Fig. 4A, 4B). Furthermore, we found an increased expression of the p-AKT in the lungs of HOCl-mice compared with PBS-mice (1.02 ± 0.10 versus 0.28 ± 0.06 AU, $p = 0.0245$; Fig. 4A, 4C). Treatment with niclosamide reduced the expression of p-AKT in the lungs of HOCl-mice compared with untreated mice (0.10 ± 0.05 versus 1.02 ± 0.10 AU, $p = 0.0029$; Fig. 4A, 4C). Moreover, expression of β-catenin in the lungs was higher in HOCl-mice than in PBS-mice (2.34 ± 0.39 versus 1.13 ± 0.32 AU, $p = 0.0379$; Fig. 4A, 4D). This expression was reduced in HOCl-mice treated by niclosamide compared with untreated mice (1.32 ± 0.16 versus 2.34 ± 0.39, $p = 0.0209$; Fig. 4A, 4D). Likewise, expression of α-SMA in the lungs was higher in HOCl-mice than in PBS-mice (2.77 ± 0.36 versus 1.19 ± 0.23 AU, $p = 0.0247$; Fig. 4A, 4E). Treatment with niclosamide reduced the expression of α-SMA in the lungs of HOCl-mice compared with untreated HOCl-mice (1.16 ± 0.12 versus 2.77 ± 0.36 AU, $p = 0.0018$; Fig. 4A, 4E). Immunohistochemistry for α-SMA and β-catenin confirmed the overexpression of these proteins in the lungs of HOCl-mice compared with the lungs of PBS-mice (Fig. 2E, 2F). Niclosamide abrogated this overexpression in treated HOCl-mice compared with untreated animals (Fig. 2E, 2F). Furthermore, production of IL-6 was higher in lungs of HOCl-mice than in the lungs of control mice (210 ± 18 versus 158 ± 10 pg/ml per mg of lung, $p = 0.0220$; Fig. 4F). Niclosamide decreased the levels of this cytokine in the lungs of HOCl-treated mice compared with untreated animals (156 ± 6 versus 210 ± 18 pg/ml per mg of lung, $p = 0.0048$; Fig. 4F).

Effects of niclosamide on T cells

Analysis of subsets of lymphocytes was performed by flow cytometry. We found a higher number of $CD4^+$ and $CD8^+$ T cells in HOCl-mice than in control mice ($CD4^+$ T cells: $13.62 \times 10^6 \pm 1.23$ versus $7.46 \times 10^6 \pm 0.26$ cells, $p = 0.0041$, Fig. 5A; $CD8^+$ T cells: $7.84 \times 10^6 \pm 0.65$ versus $5.15 \times 10^6 \pm 0.28$ cells, $p = 0.0122$, Fig. 5C). Niclosamide reduced the number of $CD4^+$ and $CD8^+$ T cells in HOCl-injected mice compared with untreated mice ($CD4^+$ T cells: $5.45 \times 10^6 \pm 0.48$ versus $13.62 \times 10^6 \pm 1.23$ cells, $p < 0.0001$, Fig. 5A; $CD8^+$ T cells: $4.09 \times 10^6 \pm 0.53 \times 10^6$ versus 7.84 ± 0.65 cells, $p = 0.0006$; Fig. 5C). Moreover, we highlighted more activated $CD4^+$ and $CD8^+$ T cells compared with control mice (activated $CD4^+$ T cells [$CD4^+CD69^+$]:

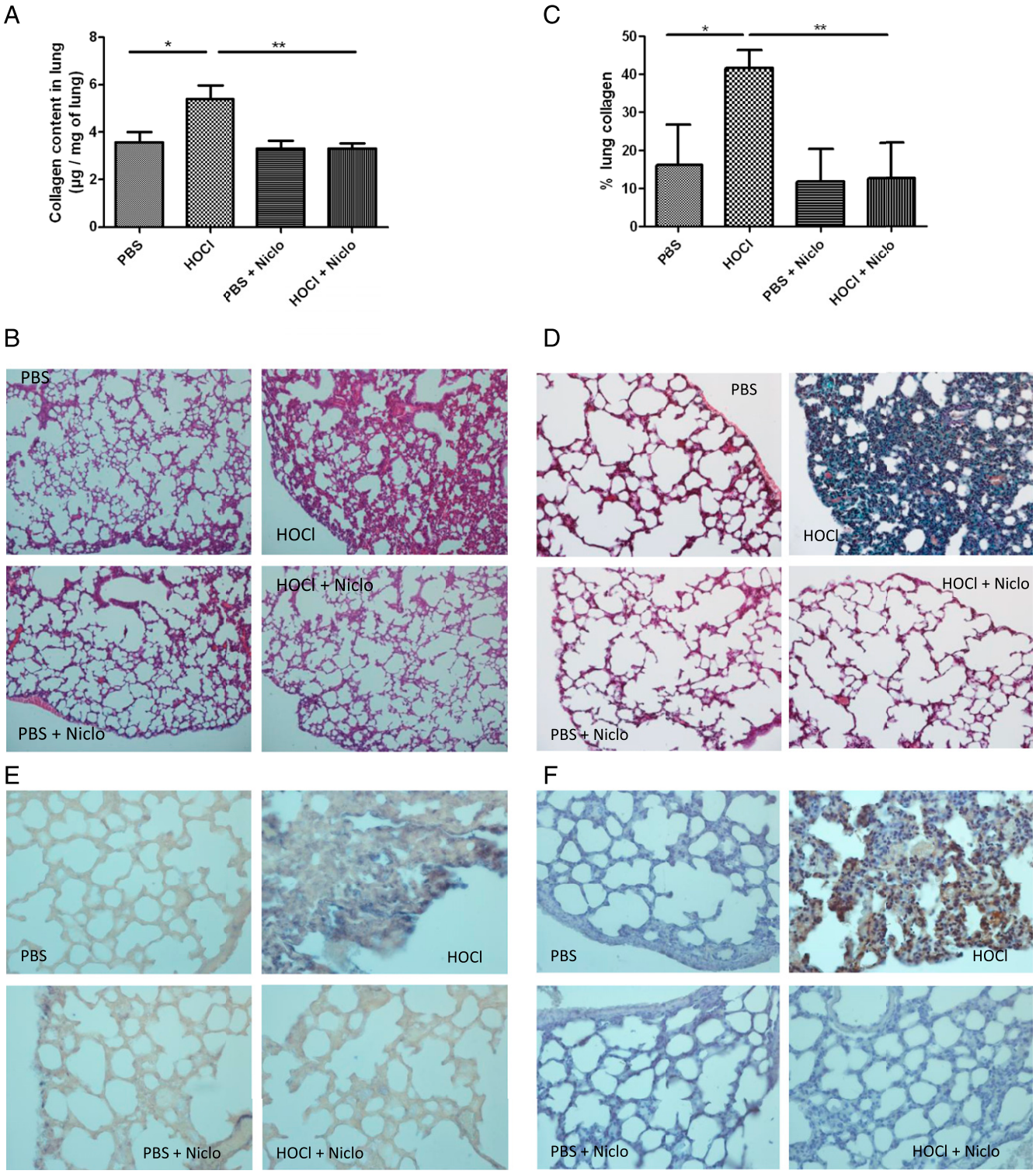

FIGURE 2. Effects of niclosamide on the lungs after SSc induction by HOCl. (**A**) Collagen content in the lungs of mice expressed in micrograms per milligram of lung. (**B**) Study of fibrosis in representative lung sections of 5 μm, in PBS-mice and HOCl-mice treated or not with niclosamide. Original magnification ×50. (**C**) Collagen content in lung of mice assessed histologically with ImageJ. (**D**) Representative 5-μm-thick sections of lung from PBS-mice and HOCl-mice, treated or not with niclosamide stained with Masson's trichrome. Original magnification ×100. (**E**). Representative sections of expression of α-SMA in the lungs of PBS-mice and HOCl-mice, treated or not with niclosamide. Original magnification ×200. (**F**). Representative sections of expression of β-catenin in the lungs of PBS-mice and HOCl-mice, treated or not with niclosamide. Original magnification ×200. Photographs were taken with a Nikon Eclipse 80i microscope. Ten mice per group representative of two experiments. (A and C) Values are means ± SEM. *$p \leq 0.05$, **$p \leq 0.01$.

$1.06 \times 10^6 \pm 0.06$ versus $0.75 \times 10^6 \pm 0.06$ cells, $p = 0.0108$, Fig. 5B; activated $CD8^+$ T cells [$CD8^+CD69^+$]: $2.34 \times 10^6 \pm 0.35$ versus $0.97 \times 10^6 \pm 0.11$ cells, $p = 0.0159$, Fig. 5D). In both $CD4^+$ and $CD8^+$ T cell populations, treatment with niclosamide reduced the number of activated cells (activated $CD4^+$ T cells: $0.64 \times 10^6 \pm 0.10$ versus $1.06 \times 10^6 \pm 0.06$ cells, $p = 0.0118$, Fig. 5B; activated $CD8^+$ T cells: $1.21 \times 10^6 \pm 0.30$ versus $2.34 \times 10^6 \pm 0.35$ cells, $p = 0.0303$, Fig. 5D).

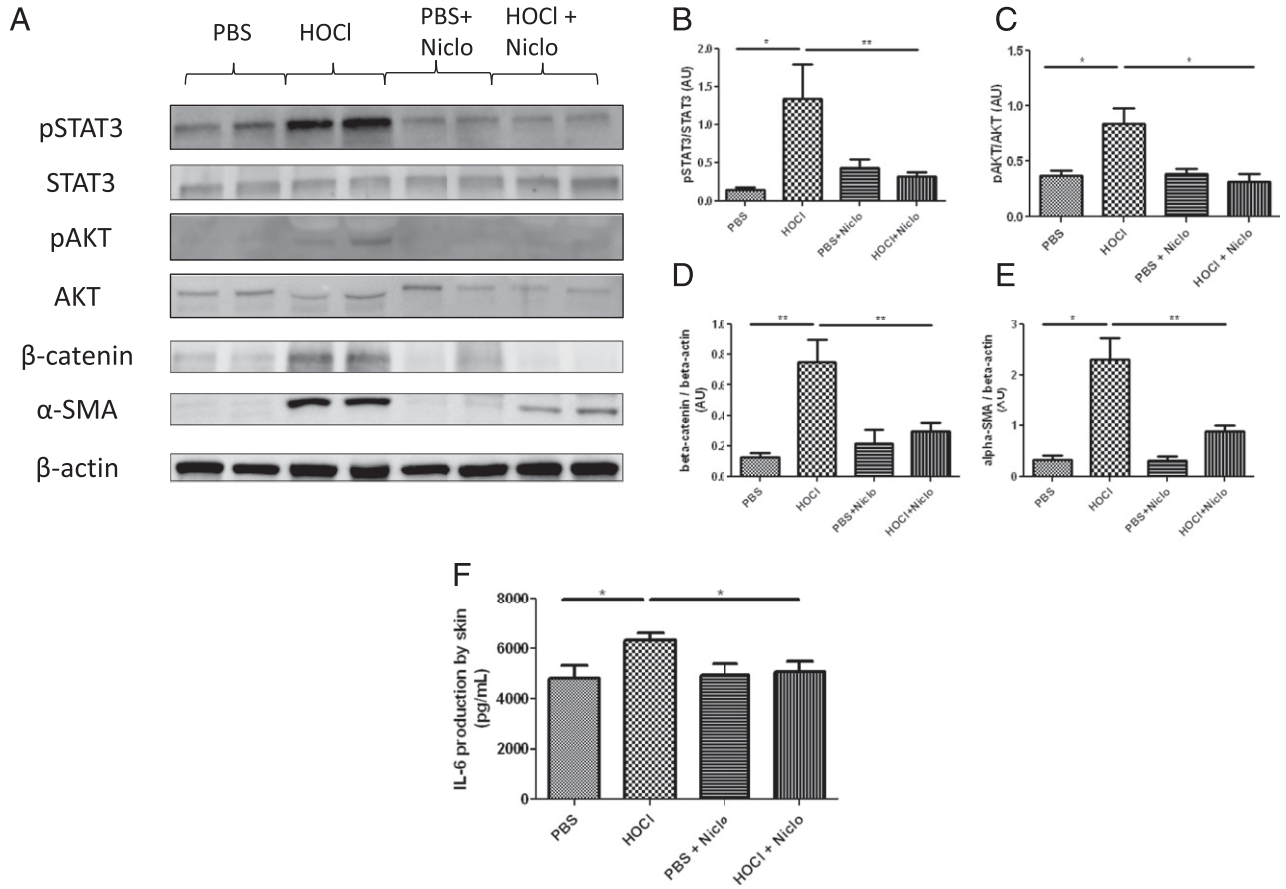

FIGURE 3. Effects of niclosamide on α-SMA, STAT3, AKT, and Wnt signaling pathways in the skin of HOCl-mice. (**A**) Representative Western blots of pSTAT3, STAT3, p-AKT, AKT, β-catenin, and α-SMA expression in the skin of PBS-mice and HOCl-mice treated or not with niclosamide. (**B**) Intensity ratio of p-STAT3 and STAT3 expression in the skin (AUs) for each mice group (n = 10 mice). (**C**) Intensity ratio of p-AKT and AKT expression in the skin (AUs) for each mice group (n = 10 mice). (**D**) Ratio of intensity of β-catenin and β-actin expression in the skin (AUs) for each mice group (n = 10 mice). (**E**) Ratio of intensity of α-SMA and β-actin expression in the skin (AUs) for each mice group (n = 10 mice). (**F**) Levels of IL-6 in the skin. Photographs were taken with a Fujifilm LAS-3000. Ten mice per group representative of two experiments. (B–F) Values are means ± SEM. *$p \leq 0.05$, **$p \leq 0.01$.

Effects of niclosamide on B cells and the production of autoantibodies

Analysis of B cells revealed more B cells in HOCl-mice compared with PBS-mice ($36.72 \times 10^6 \pm 1.94$ versus $24.54 \times 10^6 \pm 2.33$ cells, $p = 0.0039$; Fig. 6A). Treatment of diseased mice with niclosamide reduced the number of B cells ($20.13 \times 10^6 \pm 2.33$ versus $36.72 \times 10^6 \pm 1.94$ cells in HOCl-mice, $p = 0.0002$; Fig. 6A). Likewise, activated B cells ($B220^+CD69^+$) was higher in HOCl-mice than in PBS-mice ($0.69 \times 10^6 \pm 0.05$ versus $0.44 \times 10^6 \pm 0.02$ cells, $p = 0.0047$; Fig. 6B). Niclosamide decreased the number of activated B cells in HOCl-mice ($0.34 \times 10^6 \pm 0.04$ versus $0.69 \times 10^6 \pm 0.05$ cells, $p = 0.0002$; Fig. 6B). HOCl-mice developed autoantibodies directed against topoisomerase 1 (2.41 ± 0.09 versus 0.48 ± 0.03 AU in PBS-mice, $p < 0.0001$). The levels of these autoantibodies were decreased in mice treated with niclosamide (0.76 ± 0.05 versus 2.41 ± 0.09 AU, $p < 0.0001$).

Analysis of B cells populations revealed more different B cells subsets, namely, B1 ($B220^+CD43^+$), B2 ($B220^+CD43^-$), follicular ($B220^+CD43^-CD93^-CD23^+IgM^+$), and marginal zone ($B220^+CD43^-CD93^-CD23^-IgM^{high}$) B cells in HOCl-mice (B1 cells: $1.78 \times 10^6 \pm 0.12$ versus $1.22 \times 10^6 \pm 0.11$ cells in PBS-mice, $p = 0.0111$, Fig. 6C; B2 cells: $17.73 \times 10^6 \pm 1.34$ versus $11.04 \times 10^6 \pm 1.27$ cells in PBS-mice, $p = 0.0110$, Fig. 6D; follicular B cells: $13.48 \times 10^6 \pm 1.14$ versus $7.65 \times 10^6 \pm 0.60$ cells in PBS-mice, $p = 0.0098$, Fig. 6E; marginal zone B cells: $0.31 \times 10^6 \pm 0.05$ versus $0.12 \times 10^6 \pm 0.02$ cells in PBS-mice; $p = 0.0238$, Fig. 6F). Treatment by niclosamide reduced the number of cells in all of these B cells populations in HOCl-mice compared with untreated diseased mice (B1 cells: $1.01 \times 10^6 \pm 0.10$ versus $1.78 \times 10^6 \pm 0.12$ cells, $p = 0.0003$, Fig. 6C; B2 cells: $9.83 \times 10^6 \pm 1.21$ versus $13.48 \times 10^6 \pm 1.14$ cells, $p = 0.0026$, Fig. 6D; follicular B cells: $7.41 \times 10^6 \pm 0.92$ versus $7.65 \times 10^6 \pm 0.60$ cells, $p = 0.0028$, Fig. 6E; marginal zone B cells: $0.15 \times 10^6 \pm 0.02$ versus $0.31 \times 10^6 \pm 0.05$ cells; $p = 0.0104$, Fig. 6F).

Discussion

In this report, we show that HOCl-induced SSc is associated with the activation of STAT3, AKT, and Wnt/β-catenin pathways. Inhibiting these pathways with niclosamide, a drug with a well-documented safety profile, alleviates the main features of the disease, namely fibrosis, inflammation, and autoimmunity.

The HOCl-induced mouse model of SSc is characterized by skin and lung fibrosis and autoimmunity, which are classical features of the human disease. Niclosamide improves skin fibrosis as highlighted by the decrease in skin thickening, collagen content, and α-SMA expression compared with untreated diseased mice. This clinical improvement is associated with a decrease in the abnormal activation of STAT3, AKT, and Wnt/β-catenin pathways in the skin of HOCl-mice. The involvement of STAT3, AKT, and Wnt/β-catenin pathways has already been reported in skin fibrosis (19, 34, 35) but the

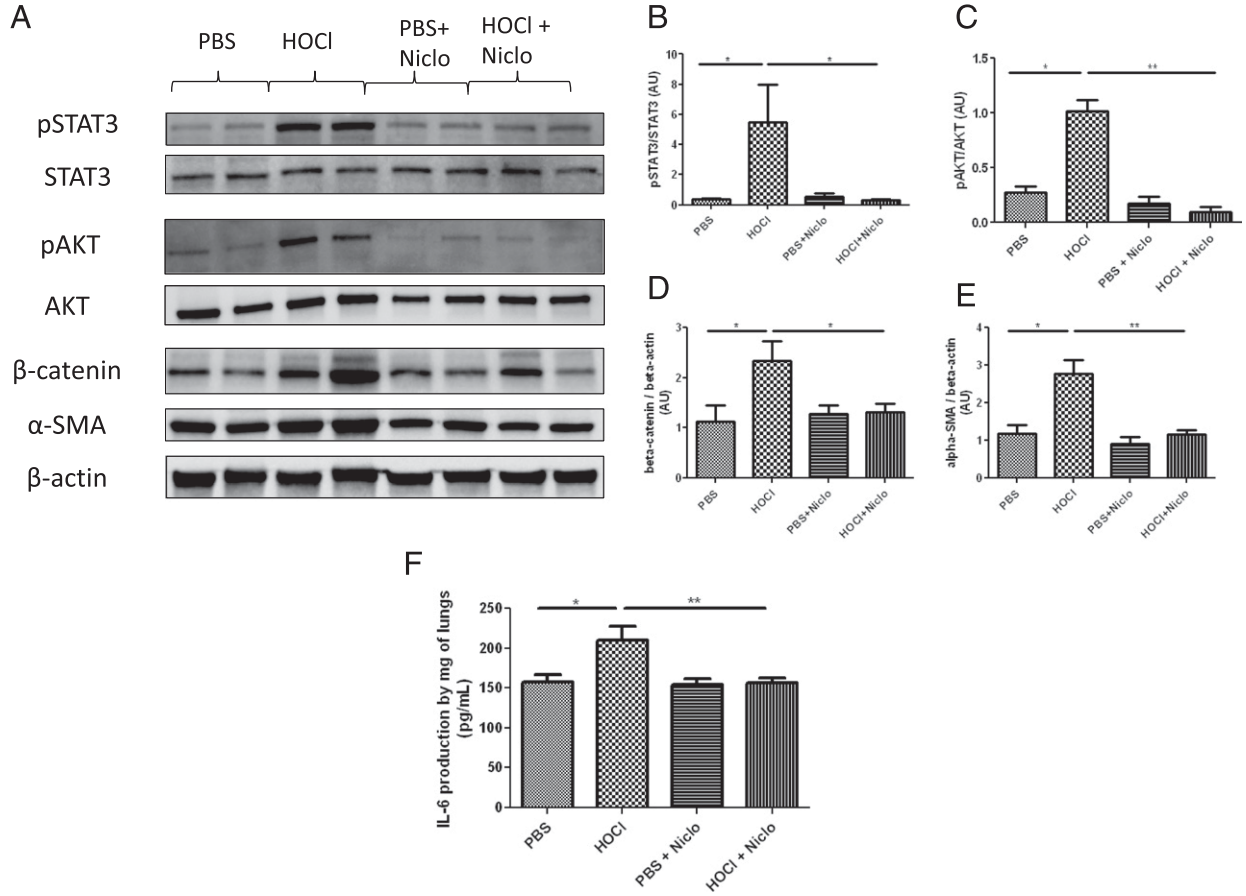

FIGURE 4. Effects of niclosamide on α-SMA, STAT3, AKT, and Wnt signaling pathways in the lungs of mice with HOCl-induced SSc. (**A**) Representative Western blots showing p-STAT3, STAT3, p-AKT, AKT, β-catenin, and α-SMA expression in the lungs of PBS-mice and HOCl-mice treated or not with niclosamide. (**B**) Ratio of intensity of p-STAT3 and STAT3 expression in the lungs (AUs) for each mice group (n = 10 mice). (**C**) Ratio of intensity of p-AKT and AKT expression in the lungs (AUs) for each mice group (n = 10 mice). (**D**) Ratio of intensity of β-catenin and β-actin expression in the lungs (AUs) for each mice group (n = 10 mice). (**E**) Ratio of intensity of α-SMA and β-actin expression in the lungs (AUs) for each mice group (n = 10 mice). (**F**) Levels of IL-6 in the lungs reported to 1 mg of lung. Photographs were taken with a Fujifilm LAS-3000. Ten mice per group representative of two experiments. (B–F) Values are means ± SEM. *$p \leq 0.05$, **$p \leq 0.01$.

consequences of their coinhibition remain to be assessed. On one hand, STAT3 triggers a transduction signal that is required for the synthesis of the extracellular matrix and cellular proliferation of fibroblasts isolated from hypertrophic scars (36). In keloids, a fibrotic disease, STAT3 promotes collagen synthesis, proliferation, and migration of fibroblasts (37, 38). Moreover, an aberrant activation of this pathway has also been reported in human sclerodermic skin and in a mouse model of SSc induced by bleomycin (19). On the other hand, the Wnt family is required for conventional wound healing (39). The Wnt/β-catenin pathway is implicated in the regulation of myeloid cell motility and adhesion during wound healing (21). In keloids and hypertrophic scars, an overexpression of Wnt signaling proteins has also been reported (40). An epigenetically altered regulation of expression of several inhibitors of Wnt signaling in keloid fibroblasts has been identified and supports the dysregulation of the Wnt/β-catenin pathway in these diseases (41, 42). This pathway is involved in the pathophysiology of different SSc models such as Tsk mice, bleomycin-induced SSc, but also in patients affected by this condition. Indeed, an activation of this pathway in dermal fibroblasts seems sufficient to cause fibrosis in mice and is associated with an upregulated expression of extracellular matrix protein-coding genes (35). As well as in keloids, epigenetic modification of the promoters of DKK1 and SFRP1 seems to contribute to aberrant Wnt signaling in SSc (43). Finally, the AKT pathway has been reported to promote fibrosis because inhibition of this pathway can reduce collagen production by human fibroblasts (26, 27). A decrease in dermal thickness, collagen content, and α-SMA in the skin of niclosamide-treated HOCl-mice corroborates the role of STAT3, AKT, and Wnt/β-catenin pathways in skin fibrosis in this model and emphasizes the therapeutic potential of coinhibitors of these pathways. Furthermore, treatment of skin fibrosis with niclosamide in bleomycin-mice supports our results because we found a decreased dermal thickness, a decreased production of hydroxyproline, and a decreased expression of β-catenin and α-SMA.

In addition, we also observed in the skin of treated HOCl-mice and treated bleomycin-mice a decrease in proinflammatory and profibrotic cytokines, such as IL-4 and IL-13, compared with untreated diseased animals. Although the activation of STAT3 was first described in Th1 lymphocytes (44), increasing evidence suggests that this pathway plays a major role in Th2 lymphocyte differentiation (45–47). The Wnt/β-catenin pathway also stimulates Th2 differentiation, as well as IL-4 and IL-13 production, in human $CD4^+$ T cells in a mouse model of allergic asthma (48, 49). Th2 differentiation and IL-4 and IL-13 overexpression is a common feature of human and mouse SSc (50, 51). Therefore, the abrogation of inflammation and cytokine production in diseased skin consecutive to STAT3 and Wnt/β-catenin inhibition by niclosamide certainly contributes to the beneficial effects on skin involvement in both of our mouse models of SSc.

Lung fibrosis in SSc remains the main cause of death in patients. In HOCl-mice, lung fibrosis is associated with overexpression of

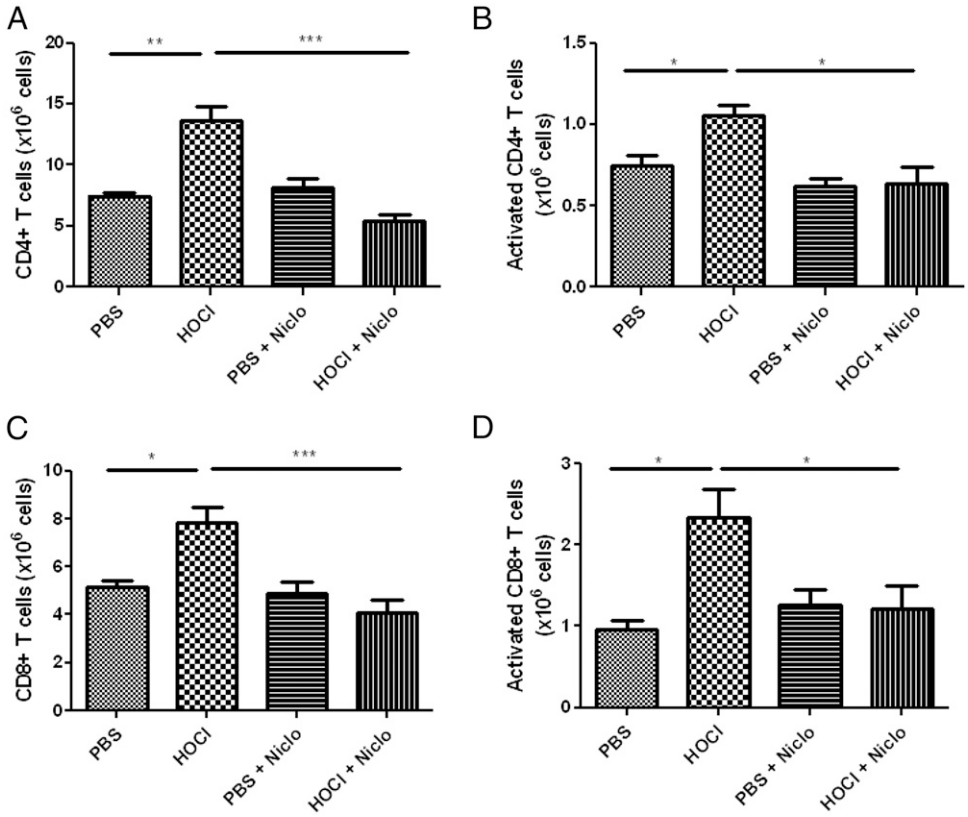

FIGURE 5. Immunological effects of niclosamide assessed by flow cytometry in mice with HOCl-induced SSc. The side scatter (SSC) and the forward scatter channels (FSC) were used to gate the leukocytes. A total of 50,000 events were accumulated for each sample. Doublets were then excluded with FSC-A and FSC-H channels. FITC (CD3) and allophycocyanin (B220) channels were used to gate T and B cells. In $CD3^+$ T cells, BV421 (CD4) and Pe-Cy7 (CD8) channels were used to gate $CD4^+$ and $CD8^+$ T cells. (**B**) $CD4^+$ and $CD8^+$ T cells, PE channel permitted to determine activated cells ($CD69^+$). Total number of each leukocyte population was calculated as: (Total number of splenocytes counted with Malassez cell for each mouse) × (% of the leukocyte population counted in the gated populations for each mouse)/100. (**A**) Splenic T $CD4^+$ cell numbers. (B) Activation of splenic T $CD4^+$ cells ($CD4^+CD69^+$). (**C**) Splenic T $CD8^+$ cell numbers. (**D**) Activation of splenic T $CD8^+$ cells ($CD8^+CD69^+$). Ten mice per group representative of two experiments. Values are the means ± SEM. $*p \leq 0.05$, $**p \leq 0.01$, $***p \leq 0.001$.

p-STAT3, p-AKT, β-catenin, and α-SMA. These pathways are involved in lung development (52, 53) and in pulmonary epithelium repair mechanisms (54). In addition, increasing evidence suggests a role of these pathways in lung fibrosis. STAT3 and AKT are hyperphosphorylated, Wnt/β-catenin pathway activated, and α-SMA overexpressed in lung fibroblasts isolated from the lungs of patients with idiopathic fibrosis (55–57). These overexpressions are associated with an overproduction of extracellular matrix and the promotion of fibroblast chemotaxis, proliferation, and differentiation (57, 58). Activation of STAT3, AKT, and Wnt/β-catenin pathways was also reported in mouse models of lung fibrosis (59, 60). STAT3 activity is directly correlated to inflammatory infiltrates in the lungs and with the severity of fibrosis (61). In our model, thickening of lung connective tissue, collagen content, and alveolar luminal narrowing, all of which are histological features of lung fibrosis, are diminished by niclosamide in HOCl-mice. Therefore, the coinhibition of STAT3, AKT and Wnt/β-catenin pathways by niclosamide targets collagen synthesis, α-SMA expression, and inflammation in the lungs and explains the improvement of lung fibrosis observed in our model.

HOCl-mice display more activated $CD4^+$ and $CD8^+$ T cells. Patients with SSc also present an abnormal activation of T and B cells (62). T cells in skin lesions are predominantly $CD4^+$ T cells. They display markers of activation and exhibit oligoclonal expansion (8, 63). Both STAT3 and Wnt/β-catenin pathways are involved in autoimmunity. Indeed, in autoimmune uveitis, STAT3 hyperphosphorylation correlates with the activation of $CD4^+$ T cells and the proliferation and survival of $CD8^+$ T cells (64, 65), whereas upregulation of Wnt/β-catenin pathway in T cells is involved in relapses (66). Furthermore, Haapaniemi et al. (67) have recently described that patients with STAT3 gain-of-function mutations present immunological disorders including autoimmunity and T lymphoproliferation, because activation of STAT3 promotes $CD4^+$ T cell proliferation and inhibits their apoptosis (68, 69). These observations strengthen the role of STAT3 in proliferation and activation of T cells and could explain the results obtained with the HOCl-induced mouse model of SSc, the increased number of over-activated $CD4^+$ and $CD8^+$ T cells, and the abrogation of this phenomenon by the inhibition of these two pathways with niclosamide.

In SSc, B cells are activated and produce autoantibodies highly characteristic of the disease (70, 71). Exposure to HOCl increased both the number and the activation of B cells but also the production of anti-DNA topoisomerase 1 autoantibodies. In SSc, cooperation between APCs and $CD4^+$ T cells is required to activate B cells and to generate autoantibodies because blockage of the CD40-CD40L interaction attenuates the severity of the disease in Tsk mice (72). STAT3 signaling in $CD4^+$ T cells is involved in the development of B cell help by $CD4^+$ T cells (73). This suggests a key role for STAT3 in the activation of B cells by $CD4^+$ T cells and the production of anti-DNA topoisomerase 1 autoantibodies. Inhibition of B-T cell cooperation by the blocking of STAT3 with niclosamide may explain the reduced activation of B cells and production of autoantibodies in niclosamide-treated HOCl-animals. In addition to its role in B-T cells cooperation,

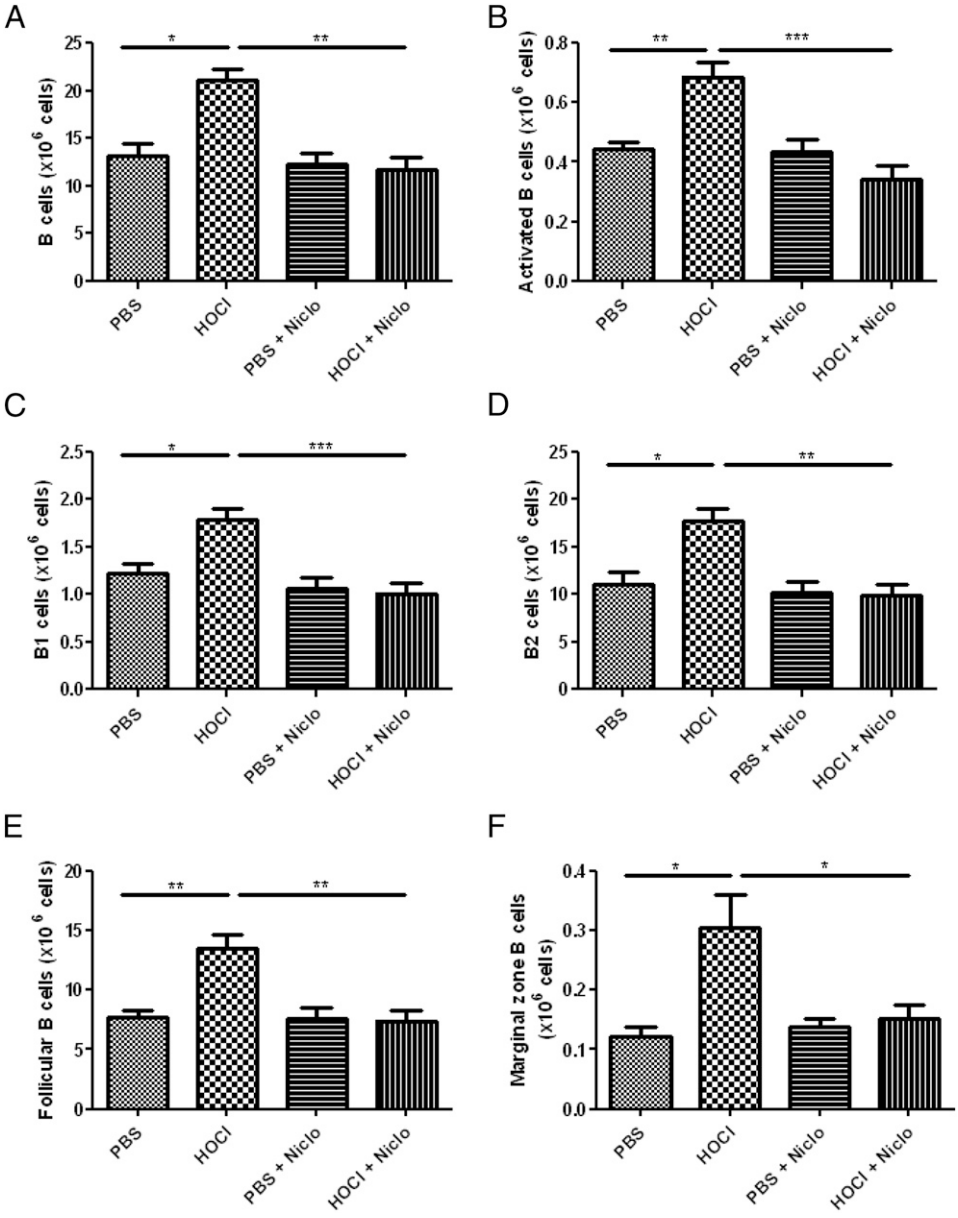

FIGURE 6. Effects of niclosamide on B cells in mice with HOCl-induced SSc assessed by flow cytometry. The side scatter (SSC) and the forward scatter channels (FSC) were used to gate the leukocytes. A total of 50,000 events were accumulated for each sample. Doublets were then excluded with FSC-A and FSC-H channels. Allophycocyanin (B220) and BV421 (CD43) channels were used to gate B1 and B2 cells. In B2 ($B220^+$ $CD43^-$) cells, PE-Cy7 (CD93) channel was used to gate mature and transitional B cells. In mature ($B220^+CD43^-CD93^-$) B cells, PerCP-Cy5.5 (IgM) and PE (CD23) permitted the gating of the marginal zone ($CD23^-IgM^{high}$) and follicular ($CD23^+IgM^+$) B cells. Total number of each leukocyte population was calculated as: (Total number of splenocytes counted with Malassez cell for each mouse) × (% of the leukocyte population counted in the gated populations for each mouse)/100. (**A**) Splenic B cell numbers. (**B**) Activation of splenic B cells, assessed by flow cytometry ($B220^+CD69^+$). (**C**) Splenic mature B1 ($B220^+CD43^+$) cell numbers. (**D**) Splenic B2 ($B220^+CD43^-$) cell numbers. (**E**) Splenic follicular B ($B220^+CD43^-CD93^-CD23^+IgM^+$) cell numbers. (**F**) Splenic marginal zone B ($B220^+CD43^-CD93^-CD23^-IgM^{high}$) cell numbers. Ten mice per group representative of two experiments. Values in are means ± SEM. $*p \leq 0.05$, $**p \leq 0.01$, $***p \leq 0.001$.

STAT3 hyperphosphorylation is triggered in follicular B2 lymphocytes upon Ag receptor engagement and may therefore contribute to the expansion of this particular B cell subset in HOCl-mice and explain the inhibition of this phenomenon by niclosamide. Furthermore, in HOCl-mice, B1 ($B220^+CD43^+$) B cells are also expanded. Although B1 cells are involved in autoimmunity (74), no evidence regarding their role in SSc has been published so far. Interestingly, a constitutive activation of STAT3 is found in normal self-renewing B1 cells (75). On the other hand, the Wnt/β-catenin pathway is involved in the regulation of proliferation and survival of B1 cells and also promotes self-renewal of these cells (76). Altogether, overactivation of these two pathways may explain the increased number of different B cell subsets observed in HOCl-animals and the abrogation of immune B cell abnormalities mediated through their inhibition upon treatment with niclosamide in HOCl-mice.

Therefore, the inhibition of STAT3, AKT, and Wnt/β-catenin pathways by niclosamide in HOCl-induced SSc in mice leads to an improvement of the disease. We observed beneficial effects of this drug on the main features of this mouse model: fibrosis, inflammation, and autoimmunity. These findings highlight the potential of niclosamide in SSc as a treatment with a well-documented safety profile.

Acknowledgments

We thank Dr. B. Weill for revising the manuscript. We also thank Muriel Andrieu and Karine Bailly of the Cochin Cytometry and Immunobiology Facility.

Disclosures

The authors have no financial conflicts of interest.

References

1. Pattanaik, D., M. Brown, B. C. Postlethwaite, and A. E. Postlethwaite. 2015. Pathogenesis of systemic sclerosis. *Front. Immunol.* 6: 272.
2. LeRoy, E. C., and T. A. Medsger, Jr. 2001. Criteria for the classification of early systemic sclerosis. *J. Rheumatol.* 28: 1573–1576.
3. Koenig, M., F. Joyal, M. J. Fritzler, A. Roussin, M. Abrahamowicz, G. Boire, J. R. Goulet, E. Rich, T. Grodzicky, Y. Raymond, and J. L. Senécal. 2008. Autoantibodies and microvascular damage are independent predictive factors for the progression of Raynaud's phenomenon to systemic sclerosis: a twenty-year

prospective study of 586 patients, with validation of proposed criteria for early systemic sclerosis. *Arthritis Rheum.* 58: 3902–3912.
4. Hinz, B., and G. Gabbiani. 2003. Cell-matrix and cell-cell contacts of myofibroblasts: role in connective tissue remodeling. *Thromb. Haemost.* 90: 993–1002.
5. Rajkumar, V. S., K. Howell, K. Csiszar, C. P. Denton, C. M. Black, and D. J. Abraham. 2005. Shared expression of phenotypic markers in systemic sclerosis indicates a convergence of pericytes and fibroblasts to a myofibroblast lineage in fibrosis. *Arthritis Res. Ther.* 7: R1113–R1123.
6. Morin, F., N. Kavian, and F. Batteux. 2015. Animal models of systemic sclerosis. *Curr. Pharm. Des.* 21: 2365–2379.
7. François, A., E. Chatelus, D. Wachsmann, J. Sibilia, S. Bahram, G. Alsaleh, and J. E. Gottenberg. 2013. B lymphocytes and B-cell activating factor promote collagen and profibrotic markers expression by dermal fibroblasts in systemic sclerosis. *Arthritis Res. Ther.* 15: R168.
8. Roumm, A. D., T. L. Whiteside, T. A. Medsger, Jr., and G. P. Rodnan. 1984. Lymphocytes in the skin of patients with progressive systemic sclerosis. Quantification, subtyping, and clinical correlations. *Arthritis Rheum.* 27: 645–653.
9. Wynn, T. A. 2004. Fibrotic disease and the T(H)1/T(H)2 paradigm. *Nat. Rev. Immunol.* 4: 583–594.
10. Steen, V. D., and T. A. Medsger. 2007. Changes in causes of death in systemic sclerosis, 1972-2002. *Ann. Rheum. Dis.* 66: 940–944.
11. Gabrielli, A., E. V. Avvedimento, and T. Krieg. 2009. Scleroderma. *N. Engl. J. Med.* 360: 1989–2003.
12. Zaazaa, H. E., M. M. Abdelrahman, N. W. Ali, M. A. Magdy, and M. Abdelkawy. 2014. Kinetic study and mechanism of Niclosamide degradation. *Spectrochim. Acta A Mol. Biomol. Spectrosc.* 132: 655–662.
13. Sack, U., W. Walther, D. Scudiero, M. Selby, D. Kobelt, M. Lemm, I. Fichtner, P. M. Schlag, R. H. Shoemaker, and U. Stein. 2011. Novel effect of antihelminthic Niclosamide on S100A4-mediated metastatic progression in colon cancer. *J. Natl. Cancer Inst.* 103: 1018–1036.
14. Li, R., S. You, Z. Hu, Z. G. Chen, G. L. Sica, F. R. Khuri, W. J. Curran, D. M. Shin, and X. Deng. 2013. Inhibition of STAT3 by niclosamide synergizes with erlotinib against head and neck cancer. *PLoS One* 8: e74670.
15. Yo, Y.-T., Y.-W. Lin, Y.-C. Wang, C. Balch, R.-L. Huang, M. W. Y. Chan, H.-K. Sytwu, C.-K. Chen, C.-C. Chang, K. P. Nephew, et al. 2012. Growth inhibition of ovarian tumor-initiating cells by niclosamide. *Mol. Cancer Ther.* 11: 1703–1712.
16. Pan, J.-X., K. Ding, and C.-Y. Wang. 2012. Niclosamide, an old antihelminthic agent, demonstrates antitumor activity by blocking multiple signaling pathways of cancer stem cells. *Chin. J. Cancer* 31: 178–184.
17. Levy, D. E., and J. E. Darnell, Jr. 2002. Stats: transcriptional control and biological impact. *Nat. Rev. Mol. Cell Biol.* 3: 651–662.
18. Tadokoro, T., Y. Wang, L. S. Barak, Y. Bai, S. H. Randell, and B. L. Hogan. 2014. IL-6/STAT3 promotes regeneration of airway ciliated cells from basal stem cells. *Proc. Natl. Acad. Sci. USA* 111: E3641–E3649.
19. Zhang, Y., C. Dees, C. Beyer, N.-Y. Lin, A. Distler, P. Zerr, K. Palumbo, L. Susok, A. Kreuter, O. Distler, et al. 2015. Inhibition of casein kinase II reduces TGFβ induced fibroblast activation and ameliorates experimental fibrosis. *Ann. Rheum. Dis.* 74: 936–943.
20. An, S. M., Q. P. Ding, and L. S. Li. 2013. Stem cell signaling as a target for novel drug discovery: recent progress in the WNT and Hedgehog pathways. *Acta Pharmacol. Sin.* 34: 777–783.
21. Amini-Nik, S., E. Cambridge, W. Yu, A. Guo, H. Whetstone, P. Nadesan, R. Poon, B. Hinz, and B. A. Alman. 2014. β-Catenin-regulated myeloid cell adhesion and migration determine wound healing. *J. Clin. Invest.* 124: 2599–2610.
22. Dees, C., and J. H. Distler. 2013. Canonical Wnt signalling as a key regulator of fibrogenesis - implications for targeted therapies? *Exp. Dermatol.* 22: 710–713.
23. Distler, A., L. Deloch, J. Huang, C. Dees, N. Y. Lin, K. Palumbo-Zerr, C. Beyer, A. Weidemann, O. Distler, G. Schett, and J. H. Distler. 2013. Inactivation of tankyrases reduces experimental fibrosis by inhibiting canonical Wnt signalling. *Ann. Rheum. Dis.* 72: 1575–1580.
24. Beyer, C., A. Schramm, A. Akhmetshina, C. Dees, T. Kireva, K. Gelse, S. Sonnylal, B. de Crombrugghe, M. M. Taketo, O. Distler, et al. 2012. β-catenin is a central mediator of pro-fibrotic Wnt signaling in systemic sclerosis. *Ann. Rheum. Dis.* 71: 761–767.
25. Distler, A., C. Ziemer, C. Beyer, N. Y. Lin, C. W. Chen, K. Palumbo-Zerr, C. Dees, A. Weidemann, O. Distler, G. Schett, and J. H. Distler. 2014. Inactivation of evenness interrupted (EVI) reduces experimental fibrosis by combined inhibition of canonical and non-canonical Wnt signalling. *Ann. Rheum. Dis.* 73: 624–627.
26. Bujor, A. M., J. Pannu, S. Bu, E. A. Smith, R. C. Muise-Helmericks, and M. Trojanowska. 2008. Akt blockade downregulates collagen and upregulates MMP1 in human dermal fibroblasts. *J. Invest. Dermatol.* 128: 1906–1914.
27. Liang, M., J. Lv, H. Chu, J. Wang, X. Chen, X. Zhu, Y. Xue, M. Guan, and H. Zou. 2014. Vertical inhibition of PI3K/Akt/mTOR signaling demonstrates in vitro and in vivo anti-fibrotic activity. *J. Dermatol. Sci.* 76: 104–111.
28. Yamaguchi, H., J. L. Hsu, and M. C. Hung. 2012. Regulation of ubiquitination-mediated protein degradation by survival kinases in cancer. *Front. Oncol.* 2: 15.
29. McCubrey, J. A., L. S. Steelman, F. E. Bertrand, N. M. Davis, S. L. Abrams, G. Montalto, A. B. D'Assoro, M. Libra, F. Nicoletti, R. Maestro, et al. 2014. Multifaceted roles of GSK-3 and Wnt/β-catenin in hematopoiesis and leukemogenesis: opportunities for therapeutic intervention. *Leukemia* 28: 15–33.
30. Kavian, N., W. Marut, A. Servettaz, C. Nicco, C. Chéreau, H. Lemaréchal, D. Borderie, N. Dupin, B. Weill, and F. Batteux. 2012. Reactive oxygen species-mediated killing of activated fibroblasts by arsenic trioxide ameliorates fibrosis in a murine model of systemic sclerosis. *Arthritis Rheum.* 64: 3430–3440.
31. Servettaz, A., C. Goulvestre, N. Kavian, C. Nicco, P. Guilpain, C. Chéreau, V. Vuiblet, L. Guillevin, L. Mouthon, B. Weill, and F. Batteux. 2009. Selective oxidation of DNA topoisomerase 1 induces systemic sclerosis in the mouse. *J. Immunol.* 182: 5855–5864.
32. Morin, F., N. Kavian, W. Marut, C. Chéreau, O. Cerles, P. Grange, B. Weill, C. Nicco, and F. Batteux. 2015. Inhibition of EGFR tyrosine kinase by erlotinib prevents sclerodermatous graft-versus-host disease in a mouse model. *J. Invest. Dermatol.* 135: 2385–2393.
33. Kavian, N., W. Marut, A. Servettaz, H. Laude, C. Nicco, C. Chéreau, B. Weill, and F. Batteux. 2012. Arsenic trioxide prevents murine sclerodermatous graft-versus-host disease. *J. Immunol.* 188: 5142–5149.
34. Jing, J., T. T. Dou, J. Q. Yang, X. B. Chen, H. L. Cao, M. Min, S. Q. Cai, M. Zheng, and X. Y. Man. 2015. Role of endothelin-1 in the skin fibrosis of systemic sclerosis. *Eur. Cytokine Netw.* 26: 10–14.
35. Hamburg-Shields, E., G. J. DiNuoscio, N. K. Mullin, R. Lafyatis, and R. P. Atit. 2015. Sustained β-catenin activity in dermal fibroblasts promotes fibrosis by up-regulating expression of extracellular matrix protein-coding genes. *J. Pathol.* 235: 686–697.
36. Ray, S., X. Ju, H. Sun, C. C. Finnerty, D. N. Herndon, and A. R. Brasier. 2013. The IL-6 trans-signaling-STAT3 pathway mediates ECM and cellular proliferation in fibroblasts from hypertrophic scar. *J. Invest. Dermatol.* 133: 1212–1220.
37. Lim, C. P., T. T. Phan, I. J. Lim, and X. Cao. 2006. Stat3 contributes to keloid pathogenesis via promoting collagen production, cell proliferation and migration. *Oncogene* 25: 5416–5425.
38. Park, G., B. S. Yoon, J. H. Moon, B. Kim, E. K. Jun, S. Oh, H. Kim, H. J. Song, J. Y. Noh, C. Oh, and S. You. 2008. Green tea polyphenol epigallocatechin-3-gallate suppresses collagen production and proliferation in keloid fibroblasts via inhibition of the STAT3-signaling pathway. *J. Invest. Dermatol.* 128: 2429–2441.
39. Carre, A. L., A. W. James, L. MacLeod, W. Kong, K. Kawai, M. T. Longaker, and H. P. Lorenz. 2010. Interaction of wingless protein (Wnt), transforming growth factor-beta1, and hyaluronan production in fetal and postnatal fibroblasts. *Plast. Reconstr. Surg.* 125: 74–88.
40. Sato, M. 2006. Upregulation of the Wnt/beta-catenin pathway induced by transforming growth factor-beta in hypertrophic scars and keloids. *Acta Derm. Venereol.* 86: 300–307.
41. Smith, J. C., B. E. Boone, S. R. Opalenik, S. M. Williams, and S. B. Russell. 2008. Gene profiling of keloid fibroblasts shows altered expression in multiple fibrosis-associated pathways. *J. Invest. Dermatol.* 128: 1298–1310.
42. Russell, S. B., J. D. Russell, K. M. Trupin, A. E. Gayden, S. R. Opalenik, L. B. Nanney, A. H. Broquist, L. Raju, and S. M. Williams. 2010. Epigenetically altered wound healing in keloid fibroblasts. *J. Invest. Dermatol.* 130: 2489–2496.
43. Dees, C., I. Schlottmann, R. Funke, A. Distler, K. Palumbo-Zerr, P. Zerr, N.-Y. Lin, C. Beyer, O. Distler, G. Schett, and J. H. W. Distler. 2014. The Wnt antagonists DKK1 and SFRP1 are downregulated by promoter hypermethylation in systemic sclerosis. *Ann. Rheum. Dis.* 73: 1232–1239.
44. Anderson, P., A. Sundstedt, L. Li, E. J. O'Neill, S. Li, D. C. Wraith, and P. Wang. 2003. Differential activation of signal transducer and activator of transcription (STAT)3 and STAT5 and induction of suppressors of cytokine signalling in T(h)1 and T(h)2 cells. *Int. Immunol.* 15: 1309–1317.
45. Mari, N., M. Hercor, S. Denanglaire, O. Leo, and F. Andris. 2013. The capacity of Th2 lymphocytes to deliver B-cell help requires expression of the transcription factor STAT3. *Eur. J. Immunol.* 43: 1489–1498.
46. Datta, A., R. Alexander, M. G. Sulikowski, A. G. Nicholson, T. M. Maher, C. J. Scotton, and R. C. Chambers. 2013. Evidence for a functional thymic stromal lymphopoietin signaling axis in fibrotic lung disease. *J. Immunol.* 191: 4867–4879.
47. El Kasmi, K. C., S. C. Pugliese, S. R. Riddle, J. M. Poth, A. L. Anderson, M. G. Frid, M. Li, S. S. Pullamsetti, R. Savai, M. A. Nagel, et al. 2014. Adventitial fibroblasts induce a distinct proinflammatory/profibrotic macrophage phenotype in pulmonary hypertension. *J. Immunol.* 193: 597–609.
48. Xue, H.-H., and D.-M. Zhao. 2012. Regulation of mature T cell responses by the Wnt signaling pathway. *Ann. N. Y. Acad. Sci.* 1247: 16–33.
49. Notani, D., K. P. Gottimukkala, R. S. Jayani, A. S. Limaye, M. V. Damle, S. Mehta, P. K. Purbey, J. Joseph, and S. Galande. 2010. Global regulator SATB1 recruits beta-catenin and regulates T(H)2 differentiation in Wnt-dependent manner. *PLoS Biol.* 8: e1000296.
50. Hasegawa, M., and K. Takehara. 2012. Potential immunologic targets for treating fibrosis in systemic sclerosis: a review focused on leukocytes and cytokines. *Semin. Arthritis Rheum.* 42: 281–296.
51. Ong, C. J., S. Ip, S. J. Teh, C. Wong, F. R. Jirik, M. J. Grusby, and H. S. Teh. 1999. A role for T helper 2 cells in mediating skin fibrosis in tight-skin mice. *Cell. Immunol.* 196: 60–68.
52. Gao, H., and P. A. Ward. 2007. STAT3 and suppressor of cytokine signaling 3: potential targets in lung inflammatory responses. *Expert Opin. Ther. Targets* 11: 869–880.
53. Beers, M. F., and E. E. Morrisey. 2011. The three R's of lung health and disease: repair, remodeling, and regeneration. *J. Clin. Invest.* 121: 2065–2073.
54. Crosby, L. M., and C. M. Waters. 2010. Epithelial repair mechanisms in the lung. *Am. J. Physiol. Lung Cell. Mol. Physiol.* 298: L715–L731.
55. Pechkovsky, D. V., C. M. Prêle, J. Wong, C. M. Hogaboam, R. J. McAnulty, G. J. Laurent, S. S. M. Zhang, M. Selman, S. E. Mutsaers, and D. A. Knight. 2012. STAT3-mediated signaling dysregulates lung fibroblast-myofibroblast activation and differentiation in UIP/IPF. *Am. J. Pathol.* 180: 1398–1412.
56. Yan, Z., Z. Kui, and Z. Ping. 2014. Reviews and prospectives of signaling pathway analysis in idiopathic pulmonary fibrosis. *Autoimmun. Rev.* 13: 1020–1025.

57. Sun, Z., C. Wang, C. Shi, F. Sun, X. Xu, W. Qian, S. Nie, and X. Han. 2014. Activated Wnt signaling induces myofibroblast differentiation of mesenchymal stem cells, contributing to pulmonary fibrosis. *Int. J. Mol. Med.* 33: 1097–1109.
58. Nagahama, K. Y., S. Togo, O. Holz, H. Magnussen, X. Liu, K. Seyama, K. Takahashi, and S. I. Rennard. 2013. Oncostatin M modulates fibroblast function via signal transducers and activators of transcription proteins-3. *Am. J. Respir. Cell Mol. Biol.* 49: 582–591.
59. Chilosi, M., V. Poletti, A. Zamò, M. Lestani, L. Montagna, P. Piccoli, S. Pedron, M. Bertaso, A. Scarpa, B. Murer, et al. 2003. Aberrant Wnt/beta-catenin pathway activation in idiopathic pulmonary fibrosis. *Am. J. Pathol.* 162: 1495–1502.
60. Kulkarni, Y. M., S. Dutta, A. K. Iyer, R. Venkatadri, V. Kaushik, V. Ramesh, C. A. Wright, O. J. Semmes, J. S. Yakisich, and N. Azad. 2016. A proteomics approach to identifying key protein targets involved in VEGF inhibitor mediated attenuation of bleomycin-induced pulmonary fibrosis. *Proteomics* 16: 33–46.
61. O'Donoghue, R. J., D. A. Knight, C. D. Richards, C. M. Prêle, H. L. Lau, A. G. Jarnicki, J. Jones, S. Bozinovski, R. Vlahos, S. Thiem, et al. 2012. Genetic partitioning of interleukin-6 signalling in mice dissociates Stat3 from Smad3-mediated lung fibrosis. *EMBO Mol. Med.* 4: 939–951.
62. Chizzolini, C., and F. Boin. 2015. The role of the acquired immune response in systemic sclerosis. *Semin. Immunopathol.* 37: 519–528.
63. Sakkas, L. I., B. Xu, C. M. Artlett, S. Lu, S. A. Jimenez, and C. D. Platsoucas. 2002. Oligoclonal T cell expansion in the skin of patients with systemic sclerosis. *J. Immunol.* 168: 3649–3659.
64. Liu, X., Y. S. Lee, C.-R. Yu, and C. E. Egwuagu. 2008. Loss of STAT3 in CD4+ T cells prevents development of experimental autoimmune diseases. *J. Immunol.* 180: 6070–6076.
65. Yu, C.-R., I. M. Dambuza, Y.-J. Lee, G. M. Frank, and C. E. Egwuagu. 2013. STAT3 regulates proliferation and survival of CD8+ T cells: enhances effector responses to HSV-1 infection, and inhibits IL-10+ regulatory CD8+ T cells in autoimmune uveitis. *Mediators Inflamm.* 2013: 359674.
66. Wildner, G., and U. Kaufmann. 2013. What causes relapses of autoimmune diseases? The etiological role of autoreactive T cells. *Autoimmun. Rev.* 12: 1070–1075.
67. Haapaniemi, E. M., M. Kaustio, H. L. M. Rajala, A. J. van Adrichem, L. Kainulainen, V. Glumoff, R. Doffinger, H. Kuusanmäki, T. Heiskanen-Kosma, L. Trotta, et al. 2015. Autoimmunity, hypogammaglobulinemia, lymphoproliferation, and mycobacterial disease in patients with activating mutations in STAT3. *Blood* 125: 639–648.
68. Durant, L., W. T. Watford, H. L. Ramos, A. Laurence, G. Vahedi, L. Wei, H. Takahashi, H.-W. Sun, Y. Kanno, F. Powrie, and J. J. O'Shea. 2010. Diverse targets of the transcription factor STAT3 contribute to T cell pathogenicity and homeostasis. *Immunity* 32: 605–615.
69. van der Fits, L., M. S. van Kester, Y. Qin, J. J. Out-Luiting, F. Smit, W. H. Zoutman, R. Willemze, C. P. Tensen, and M. H. Vermeer. 2011. MicroRNA-21 expression in CD4+ T cells is regulated by STAT3 and is pathologically involved in Sézary syndrome. *J. Invest. Dermatol.* 131: 762–768.
70. Sato, S., M. Fujimoto, M. Hasegawa, K. Takehara, and T. F. Tedder. 2004. Altered B lymphocyte function induces systemic autoimmunity in systemic sclerosis. *Mol. Immunol.* 41: 1123–1133.
71. Tyndall, A., and S. Fistarol. 2013. The differential diagnosis of systemic sclerosis. *Curr. Opin. Rheumatol.* 25: 692–699.
72. Komura, K., M. Fujimoto, K. Yanaba, T. Matsushita, Y. Matsushita, M. Horikawa, F. Ogawa, K. Shimizu, M. Hasegawa, K. Takehara, and S. Sato. 2008. Blockade of CD40/CD40 ligand interactions attenuates skin fibrosis and autoimmunity in the tight-skin mouse. *Ann. Rheum. Dis.* 67: 867–872.
73. Ysebrant de Lendonck, L., F. Eddahri, Y. Delmarcelle, M. Nguyen, O. Leo, S. Goriely, and A. Marchant. 2013. STAT3 signaling induces the differentiation of human ICOS(+) CD4 T cells helping B lymphocytes. *PLoS One* 8: e71029.
74. Martin, F., and J. F. Kearney. 2001. B1 cells: similarities and differences with other B cell subsets. *Curr. Opin. Immunol.* 13: 195–201.
75. Karras, J. G., Z. Wang, L. Huo, R. G. Howard, D. A. Frank, and T. L. Rothstein. 1997. Signal transducer and activator of transcription-3 (STAT3) is constitutively activated in normal, self-renewing B-1 cells but only inducibly expressed in conventional B lymphocytes. *J. Exp. Med.* 185: 1035–1042.
76. Novo, M. C. T., L. Osugui, V. O. dos Reis, I. M. Longo-Maugéri, M. Mariano, and A. F. Popi. 2015. Blockage of Wnt/β-catenin signaling by quercetin reduces survival and proliferation of B-1 cells in vitro. *Immunobiology* 220: 60–67.